Binding Mechanism of Nonspecific Lipid Transfer Proteins and Their Role in Plant Defense †

ARTICLE *in* BIOCHEMISTRY · DECEMBER 2004

Impact Factor: 3.02 · DOI: 10.1021/bi048873j · Source: PubMed

7 AUTHORS, INCLUDING:

Dharmaraj Samuel
Gilead Sciences
23 PUBLICATIONS **709** CITATIONS
SEE PROFILE

Ping-Chiang Lyu
National Tsing Hua University
147 PUBLICATIONS **3,232** CITATIONS
SEE PROFILE

Articles

Binding Mechanism of Nonspecific Lipid Transfer Proteins and Their Role in Plant Defense†

Chao-Sheng Cheng, Dharmaraj Samuel,§ Yaw-Jen Liu, Je-Chyi Shyu, Szu-Ming Lai, Ku-Feng Lin, and Ping-Chiang Lyu*

Department of Life Sciences, National Tsing Hua University, Hsinchu 30043, Taiwan

Received June 2, 2004; Revised Manuscript Received August 10, 2004

ABSTRACT: Plant nonspecific lipid transfer proteins (nsLTPs) are small basic proteins that transport phospholipids between membranes. On the basis of molecular mass, nsLTPs are subdivided into nsLTP1 and nsLTP2. NsLTPs are all helical proteins stabilized by four conserved disulfide bonds. The existence of an internal hydrophobic cavity, running through the molecule, is a typical characteristic of nsLTPs that serves as the binding site for lipid-like substrates. NsLTPs are known to participate in plant defense, but the exact mechanism of their antimicrobial action against fungi or bacteria is still unclear. To trigger plant defense responses, a receptor at the plant surface needs to recognize the complex of a fungal protein (elicitin) and ergosterol. NsLTPs share high structural similarities with elicitin and need to be associated with a hydrophobic ligand to stimulate a defense response. In this study, binding of sterol molecules with rice nsLTPs is analyzed using various biophysical methods. NsLTP2 can accommodate a planar sterol molecule, but nsLTP1 binds only linear lipid molecules. Although the hydrophobic cavity of rice nsLTP2 is smaller than that of rice nsLTP1, it is flexible enough to accommodate the voluminous sterol molecule. The dissociation constant for the nsLTP2/cholesterol complex is approximately 71.21 μM as measured by H/D exchange and mass spectroscopic detection. Schematic models of the nsLTP complex structure give interesting clues about the reason for differential binding modes. Comparisons of NMR spectra of the sterol/rice nsLTP2 complex and free nsLTP2 revealed the residues involved in binding.

Plant nonspecific lipid transfer proteins (nsLTPs)[1] have been purified from various sources such as wheat, maize, apricot, rice, and others (*1*−*3*). NsLTPs are classified into two subfamilies according to their molecular masses: nsLTP1 (9 kDa) and nsLTP2 (7 kDa) (*3*, *4*). Structures of nsLTPs have been solved with NMR and X-ray diffraction methods. The three-dimensional fold of nsLTP1 is composed of four α-helices and a flexible stretch of C-terminal residues (*5*−*7*). The three-dimensional structure of nsLTP2 consists of a rigid helical portion and a flexible unstructured portion (*8*, *9*). All nsLTPs are stabilized by four disulfide bonds despite their different patterns in nsLTP1 and nsLTP2 (*2*). The major structural difference of nsLTP1 and nsLTP2 is in the hydrophobic cavity. The hydrophobic cavity, the binding site for hydrophobic ligands, is smaller in nsLTP2 compared to nsLTP1 (*6*, *7*, *10*).

NsLTPs facilitate in vitro transport of lipids (*11*, *12*). These proteins also participate in biosynthesis of the cutin layer and surface wax through transport of acyl monomers. A remarkable property of nsLTPs is their involvement in plant defense, although the exact mechanism of antimicrobial actions against fungi or bacteria is still unclear (*13*−*15*). A class of fungal pathogens from *Phytophthora* or *Pythium* genera (Oomycetes), unable to synthesize sterol molecules for their life cycle, capture them from the membrane of the invaded plants (*16*−*18*). Sterol is one of the major components in membranes that regulate the membrane fluidity and permeability (*19*). Pathogens secret elicitins that act as a shuttle to capture sterol from the plant surface required for the active phases of sexual and asexual reproduction (*20*). Elicitin/ergosterol complexes can be recognized by specific receptors on the plant membrane surface and trigger the plant defense responses. For example, β-cryptogein, a small holoprotein of the elicitin family, captures essential sterol (ergosterol) for the *Phytophthora* fungus. Cryptogein, a ∼10 kDa protein containing three disulfides, shares similar structural motifs with nsLTPs. Cryptogein needs to form a complex with a sterol molecule to trigger the plant defense mechanism (*21*). Although endogenous nsLTP1 binds the

† This work was supported in part by Research Grant NSC-923112B007006/932311B007012 from the National Science Council, Taiwan, and a Program for Promoting Academic Excellence of Universities grant (91-B-FA05-1-4) from the Ministry of Education, Taiwan.

§ Current address: Basic Science Division, Fox Chase Cancer Center, 333 Cotman Ave, Philadelphia, PA 19111.

* To whom correspondence should be addressed. Phone: +886 35722762. Fax: +886 35715934. E-mail: pclyu@life.nthu.edu.tw.

[1] Abbreviations: nsLTPs, nonspecific lipid transfer proteins; RMSD, root-mean-square deviation; GdnHCl, guanidine hydrochloride; ANS, 8-anilino-1-naphthalenesulfonic acid; NMR, nuclear magnetic resonance spectroscopy.

10.1021/bi048873j CCC: $27.50
Published on Web 09/29/2004

plant receptor recognized by exogenous fungal proteins (elicitins), it fails to trigger plant defense responses (*20*, *22*). Recently, a putative lipid transfer protein (nsLTP2) involved in plant defense in *Arabidopsis* was identified (*23*). A recent review of nsLTP roles in plant defense suggested that a hydrophobic ligand needs to bind with this protein to induce plant defense (*20*). Moreover, sterol molecules such as ergosterol or cholesterol can also promote nsLTP mRNA accumulation (*24*). On the basis of these observations, binding of sterol molecules to nsLTPs was explored using various spectroscopic techniques such as fluorescence, circular dichroism, mass spectrometry, and NMR.

EXPERIMENTAL PROCEDURES

Materials. Rice nsLTPs were extracted from rice seeds according to the procedure described previously (*4*, *25*). The protein purity was confirmed using a Micromass Quattro Ultima with the electron spray ionization (ESI-MASS) method. 8-Anilino-1-naphthalenesulfonic acid (ANS), ergosta-5,7,9(11),22-tetraen-3β-ol (dehydroergosterol, DHE), 5-cholesten-3β-ol (cholesterol), 1-myristoyl-*sn*-glycero-3-phosphocholine (LysoPC14), and guanidine hydrochloride (Gdn·HCl) were purchased from Sigma Co. The concentration of dehydroergosterol was estimated using its molar extinction coefficient (*26*). Deuterium oxide was purchased from Cambridge Isotope Laboratories, Inc. All the chemicals used were of high-quality analytical grade.

Fluorescence Binding Assay. Interaction kinetics were measured as previously described (*18*). A 1.067 μM concentration of nsLTPs was added to a cuvette containing 0.5 μL of dehydroergosterol (0.4 mM) in 30 mM phosphate buffer solution (pH 7.2). The fluorescence intensity was monitored at 370 nm (λ_{ex} = 325 nm) using an SLM 48000S spectrofluorometer at 298 K. ANS was also used to study the competitive interaction of dehydroergosterol or LysoPC14 with nsLTPs. ANS (25 μM) was added to a solution containing nsLTPs (0.8 μM) in 30 mM phosphate buffer (pH 7). Dehydroergosterol (2 μM) or LysoPC14 (2 μM) was then added, and the fluorescence intensity was recorded for 1500 s. The fluorescence intensity was monitored at 490 nm (λ_{ex} = 365 nm). The protein solution (10 μM) in 30 mM phosphate buffer was titrated with a small amount of cholesterol (5 μL) via monitoring the fluorescence intensity on a Perkin-Elmer LS 55 luminescence spectrometer at 298 K. The excitation and the emission wavelengths were set to 275 and 305 nm, respectively. Data points on the titration curves were an average of three measurements.

Circular Dichroism (CD) Experiments. nsLTP2 (15 μM) and cholesterol in an equimolar ratio were incubated at room temperature overnight. The protein stability was measured using Gdn·HCl-induced denaturation. Protein or protein/ligand solutions (300 μL) containing 30 mM phosphate buffer (pH 7.0) were treated with various concentrations of Gdn·HCl. The reversibility of the protein folding was confirmed by diluting the denaturant in protein solutions (8 M) to lower concentrations of Gdn·HCl. A final protein concentration of 15 μM in 30 mM phosphate buffer (pH 7.0) was maintained for all the refolding experiments. CD spectra were recorded with an Aviv 202 spectropolarimeter at 1 nm resolution using a 1 mm path length cuvette. An average of three CD scans, measured at 298 K in the far-UV region between 210 and 250 nm, was used to determine the α-helical content of the protein. The solvent-subtracted spectra were converted to the mean residue ellipticity [θ] (MRE) in deg·cm^2·dmol^{-1} from the ellipticity values in millidegrees (θ). The fraction of helix (f) was calculated using the equation $f = [(-[\theta]_{obs}/40000(n - 4))/n] \times 100$, where $[\theta]_{obs}$ and n refer to the observed ellipticity value and number of amino acids, respectively (*27*).

Hydrogen/Deuterium Exchange. NsLTP2 was dissolved in water to a final concentration of 0.4 mM (pH 7.0). An eqimolar ratio of cholesterol in ethanol was added and incubated with protein solution overnight. Subsequently, D_2O was added to aqueous solutions of nsLTP2 and the nsLTP2/sterol complex in a 1:50 (H_2O:D_2O) ratio to initiate the H/D exchange. After different incubation times, the H/D exchange was quenched by adding ice-cold formic acid solution (ACN/H20/formic acid (50:49:1)). The samples were immediately analyzed with ESI-MS (*28*, *29*). Different amounts of cholesterol, at molar ratios (sterol:protein) from 0 to 10, were incubated with a rice nsLTP2 solution (0.4 mM) for the titration experiment. The H/D exchange was allowed for 100 min and quenched as described above. The dissociation constant value was estimated from the changes in deuterium content upon titrating nsLTP2 with a given cholesterol, using the nonlinear relation

$$F = F_0 + [(F_s - F_0)/2][(K_d/P_t + R_i/(n+1)) - ((K_d/P_t + R_i/(n+1))^2 - 4R_i/n)^{0.5}]$$

where F_0 and F_s represent the number of H atoms exchanged to D in the absence and presence of saturating concentrations of the ligand (cholesterol), P_t is the total concentration of the protein, R_i are various molar ratios of cholesterol with rice nsLTP2, and K_d is the dissociation constant of the protein/cholesterol complex (*30*). Each data point was an average of three experiments. The curve fitting of the titration data was created using KaleidaGraph (Synergy Software).

Mass measurements in positive ion mode were performed on a Micro Mass Quattro Ultima mass spectrometer by the ESI-MASS method. The cone voltage and capillary voltage were 55 V and 3.5kV, respectively. Nitrogen gas was used to evaporate the solvent from the charged droplets. The HPLC system used was an Agilent 1100 series with a liquid chromatograph/mass-selective detector (LC/MSD). The sample was eluted with a 20 μL/min isocratic flow of 50% ACN, 49% H_2O, and 1% formic acid.

Nuclear Magnetic Resonance Experiments. Rice nsLTP2 ($\sim$3 mM) was dissolved in 50 mM phosphate buffer (90% H_2O and 10% D_2O, pH 6.4) containing sodium 3-(trimethylsilyl)-[2,2,3,3-^{2}H]propionate (d_4-TSP) as the internal standard (*8*). A sufficient amount of cholesterol was added to form a protein/cholesterol complex (*31*, *32*). The nsLTP2/cholesterol complex was prepared by adding cholesterol to the nsLTP2 solution for overnight incubation. The solution containing the complex was lyophilized and redissolved to maintain the same buffer conditions. The solution was centrifuged to remove any suspended particles. NMR experiments were carried out on a Bruker 600 MHz NMR spectrometer. Two-dimensional TOCSY spectra were obtained with 2048 complex data points in the detection period (t2) and 512 points in the evolution period (t1) at 298 K. The total numbers of scans and dummy scans were 48 and 16, respectively. NMR spectra were processed using XWIN-

nmr (Bruker) and analyzed using SPARKY (*33*). The difference in chemical shift perturbations were calculated using the equation $\Delta\delta(^{\alpha}H,^{N}H) = |\Delta\delta(^{\alpha}H)| + |\Delta\delta(^{N}H)|$. $^{\alpha}H$ and ^{N}H represent amide and α protons, respectively (*34*, *35*).

Docking. A computer program, Gramm compiled in Mandrake 8.0 Linux platform, was used to dock ergosterol and cholesterol (*36*−*38*). All the possible positions and orientations of ligand were tried with the geometric and hydrophobic docking modes. In the intermolecular energy calculation, the repulsion potential and attraction double range were set according to the user manual. The grid step was set to 1.7 Å. The complex structure was further refined with the energy minimization protocol in the steepest descent method in the Discover 3 module of the InsightII package (Accelrys Inc.) (*39*). A stable final conformation was attained after CVFF force-field energy minimization (500 steps) with a dielectric constant value equal to 1.0. Various interactions involved in the protein/ligand complex were established using Ligplot v.4.0 (*40*). The hydrophobic cavity volume was calculated using Voidoo in van der Waals mode with a 1.0 Å probe radius and a 1.1 unit of van der Waals growth factor (*41*). The electronic potential surface map of the protein was calculated using Grasp (*42*).

RESULT AND DISCUSSION

Fluorescence Binding Assay. Sterol binding to nsLTPs was explored using a cholesterol analogue with intrinsic fluorescence, DHE. Fluorescence intensity (a measure of interaction kinetics) of the solution containing rice nsLTP2 and DHE was gradually increased, but the intensity was not altered for the solution containing rice nsLTP1 and DHE (Figure 1A). The results demonstrated that rice nsLTP2 could bind to the sterol molecule but not nsLTP1. This was further confirmed with a competitive binding experiment with an extrinsic fluorophore, ANS. ANS is known to bind hydrophobic protein surfaces. DHE or LysoPC14 was added to preequilibrated complex (ANS/protein) solutions to compete with ANS (Figure 1B). Addition of DHE did not change the fluorescence intensity in an ANS/rice nsLTP1 complex. In other words, DHE failed to replace ANS to bind with rice nsLTP1. Inversely, the fluorescence intensity of the solution containing the rice nsLTP2/ANS complex decreased upon DHE addition. The decrease in the fluorescence intensity was due to replacement of ANS by DHE in the hydrophobic cavity of rice nsLTP2. In the same way, addition of LysoPC14 can change the fluorescence intensity in two ANS/protein complexes (Figure 1B). Both rice nsLTPs are able to bind the linear lipid molecule LysoPC14.

CD Experiments. The chemical denaturation method was used to estimate the stabilities of native and cholesterol-bound states of nsLTP2. A denaturant-induced unfolding study at increasing concentrations of Gdn·HCl monitored by CD showed a marginal stability increase for the ligand-bound form (Figure 2). A perfect overlap of unfolding and refolding profiles revealed that protein denatures reversibly (*43*, *44*). Nonlinear least-squares regression was used to analyze these unfolding data according to a two-state model using the linear extrapolation method (*45*, *46*). The concentration of the denaturant at which 50% of the protein is unfolded (C_m) for cholesterol-bound rice nsLTP2 (4.14 M) was slightly higher than that for free rice nsLTP2 (3.89 M). Similarly, the free

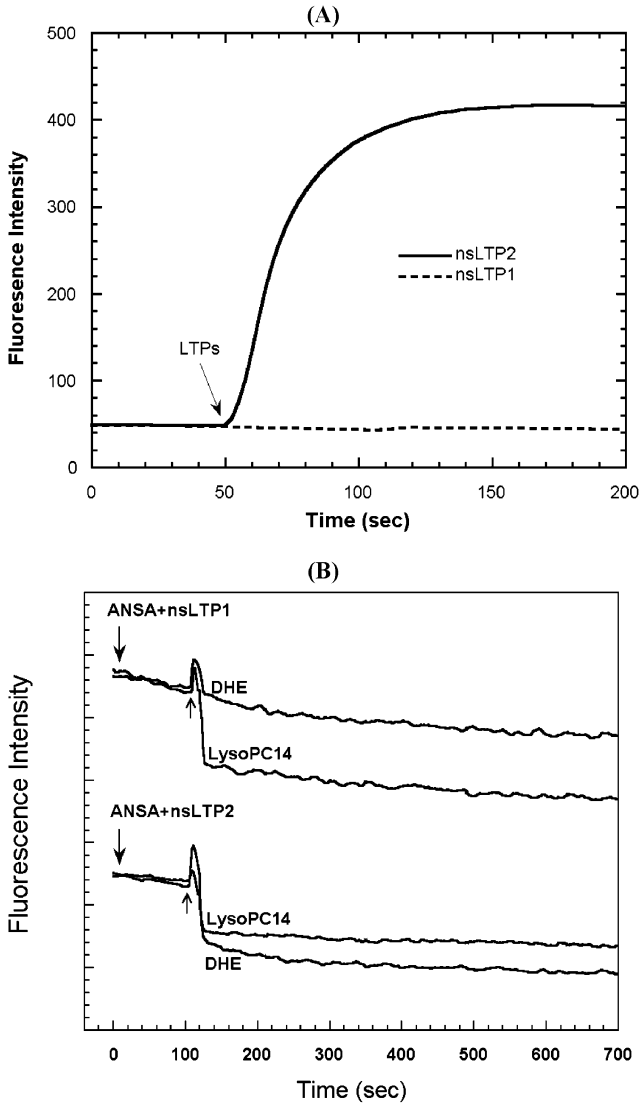

FIGURE 1: (A) Association kinetics of DHE with rice nsLTP1 (---) and nsLTP2 (—). Protein was added to DHE solutions at 50 s, indicated with an arrow. The fluorescence intensity of DHE increased upon nsLTP2 addition. The fluorescence intensity was monitored at 370 nm with excitation at 325 nm at 298 K. (B) Competitive experiment between ANS and DHE/LysoPC14. An extrinsic fluorophore, ANS, was used to monitor DHE/LysoPC14 binding with rice nsLTPs. After equilibration of the ANS/protein complex (∼100 s, indicated with an arrow), DHE or LysoPC14 was added to compete with ANS. The fluorescence intensity was recorded at 490 nm; the excitation wavelength was set to 365 nm.

energies of unfolding ($\Delta G^{\circ}_{H_2O}$) for free and ligand-bound states of nsLTP2 were 14.568 and 16.865 kJ mol^{-1}, respectiely.

Hydrogen/Deuterium Exchange. Hydrogen/deuterium exchange is slower in the more protected regions of a protein containing secondary structural elements (α-helices and *β*-sheets) (*47*−*49*). In contrast, exchange rates in the less protected regions (N-terminus, C-terminus, surface, or loops) are enhanced. The kinetics of deuterium uptake for rice nsLTP2 and the nsLTP2/cholesterol complex were analyzed using mass spectroscopic techniques (Figure 3A). The deuterium uptake rates were fast in the first 30 min, where the overall deuterium contents for the free and cholesterol complex forms of nsLTP2 were 87 and 79, respectively. The H/D exchange became relatively slower at longer incubation time, where the total numbers of exchangeable hydrogens

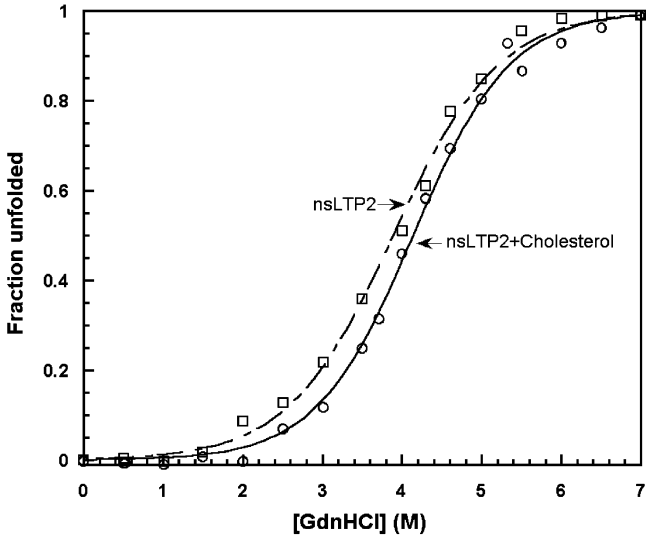

FIGURE 2: Gdn·HCl-induced unfolding curves of the cholesterol-bound and free forms of nsLTP2. Unfolding was monitored at different Gdn·HCl concentrations at 298 K. The protein stability (C_m and ΔG) was estimated according to a two-state model (a sigmoid curve). The square symbols represent protein alone, while the circle symbols are for the complex.

were 94 for free nsLTP2 and 87 for the complex. Even after a few days of incubation, the overall deuterium uptake remained constant.

NsLTP2 titrated with various molar ratios of sterol molecules was used to determine the dissociation constant (K_d) (Figure 3B). The number of hydrogens swapped with deuterium decreased with increasing cholesterol concentration and attained a constant value, approximately 78. Lesser deuterium substitution indicated that cholesterol-bound nsLTP2 forms a tight and less solvent exposed structure. The titration curve was fit to a 1:1 binding model, resulting in a dissociation constant (K_d) of 71.21 μM.

Nuclear Magnetic Resonance Experiments. Atomic level information of ligand/protein interactions can be obtained from nuclear magnetic resonance (NMR) methods. The sterol binding resulted in upfield chemical shift perturbations in the one-dimensional ^{1}H NMR spectrum (data not shown). These changes may be caused by aromatic ring current shifts, resulting in changes of up to 1.5 ppm for methyl groups of the protein that contact the sterol ring structure, or may be the signals from sterol itself. These interactions may also alter protein flexibility, causing other chemical shift effects. Homonuclear two-dimensional TOCSY spectra of free nsLTP2 and the cholesterol/nsLTP2 complex were compared to locate the interacting residues. The fingerprint regions of the two spectra were assigned with the help of previously published chemical shift values (Figure 4A) (*34*, *35*). The assignments were also cross-checked and confirmed by their spin patterns (*50*). None of the protein residues showed significant chemical shift perturbations, indicating that cholesterol binding did not alter the overall protein structure (*34*, *35*). However, chemical shift perturbations ($\Delta\sigma > 0.018$ ppm shown with a dashed line) were observed for a few residues (Figure 4B). Asn^4, Ala^5, Gln^7, Leu^8, Thr^9, Ile^{15}, Gly^{18}, Phe^{36}, Cys^{37}, Phe^{39}, Lys^{41}, Tyr^{45}, Arg^{47}, Tyr^{48}, Val^{49}, Asn^{50}, Ser^{51}, Arg^{55}, and Val^{58} are the residues exhibiting changes in their chemical environment upon sterol binding (represented with bold letters in the protein sequence, Figure

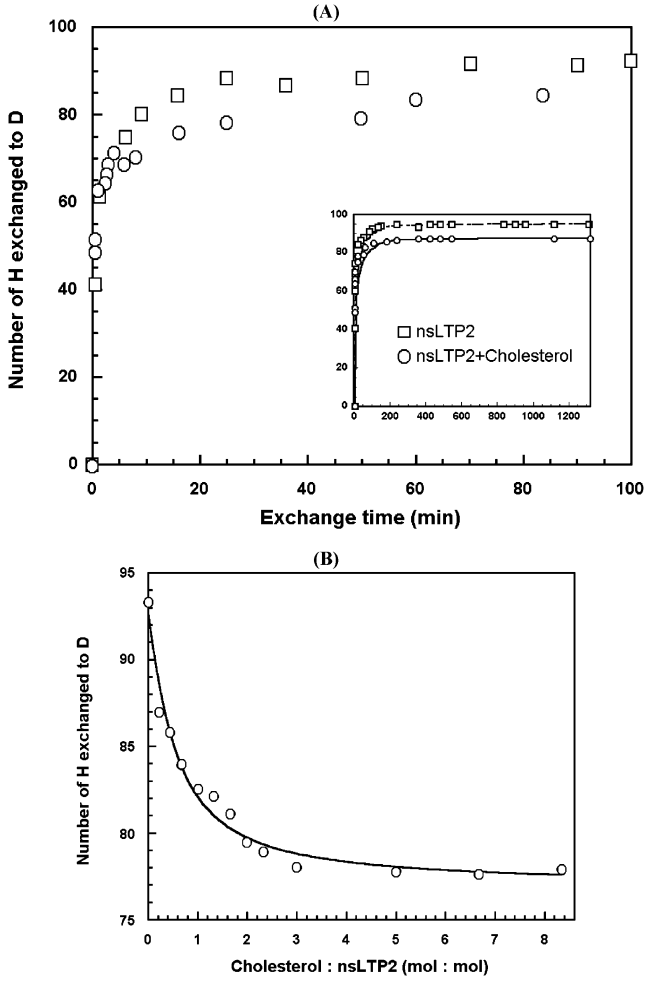

FIGURE 3: (A) Number of H/D exchanges of rice nsLTP2 in the free and cholesterol-bound states represented as a function of incubation time (0−100 min). The inset figure elucidates the deuterium uptake for 24 h of incubation. H/D exchanges at various time intervals of the free and complex forms of protein are represented by squares and circles, respectively. (B) H/D exchange monitored at various molar ratios of cholesterol with rice nsLTP2. Each data point was measured after 100 min of incubation.

4B). A schematic diagram of secondary structure elements for rice nsLTP2 is also shown at the bottom of Figure 4B, with helices represented by cylinders. The residues involved in sterol binding are colored green in the three-dimensional structure of rice nsLTP2 (Figure 5). The disulfide bonds are shown in yellow, while the protein backbone is represented by a tube. The major conformational changes upon sterol binding occurred around helices I, IV, and V. A small set of new peaks appearing in the fingerprint region of the complex spectrum may arise from the bound sterol molecule.

Docking of a Sterol Molecule with Rice nsLTPs. As a preliminary step to understanding the role of sterol/protein complexes in plant defense mechanisms, ergosterol and cholesterol were docked with rice nsLTPs (PDB codes 1RZL for nsLTP1 and 1L6H for nsLTP2) using the Gramm program (*36*−*38*). All the possible positions and orientations of ligand in the proteins were attempted. Our docking results showed that ergosterol and cholesterol cannot be fit into the hydrophobic cavity of rice nsLTP1 (data not shown). The hydrophobic docking mode gave a reasonable result for the rice nsLTP2/sterol complexes. Cholesterol and ergosterol acted through the same binding site at the hydrophobic cavity

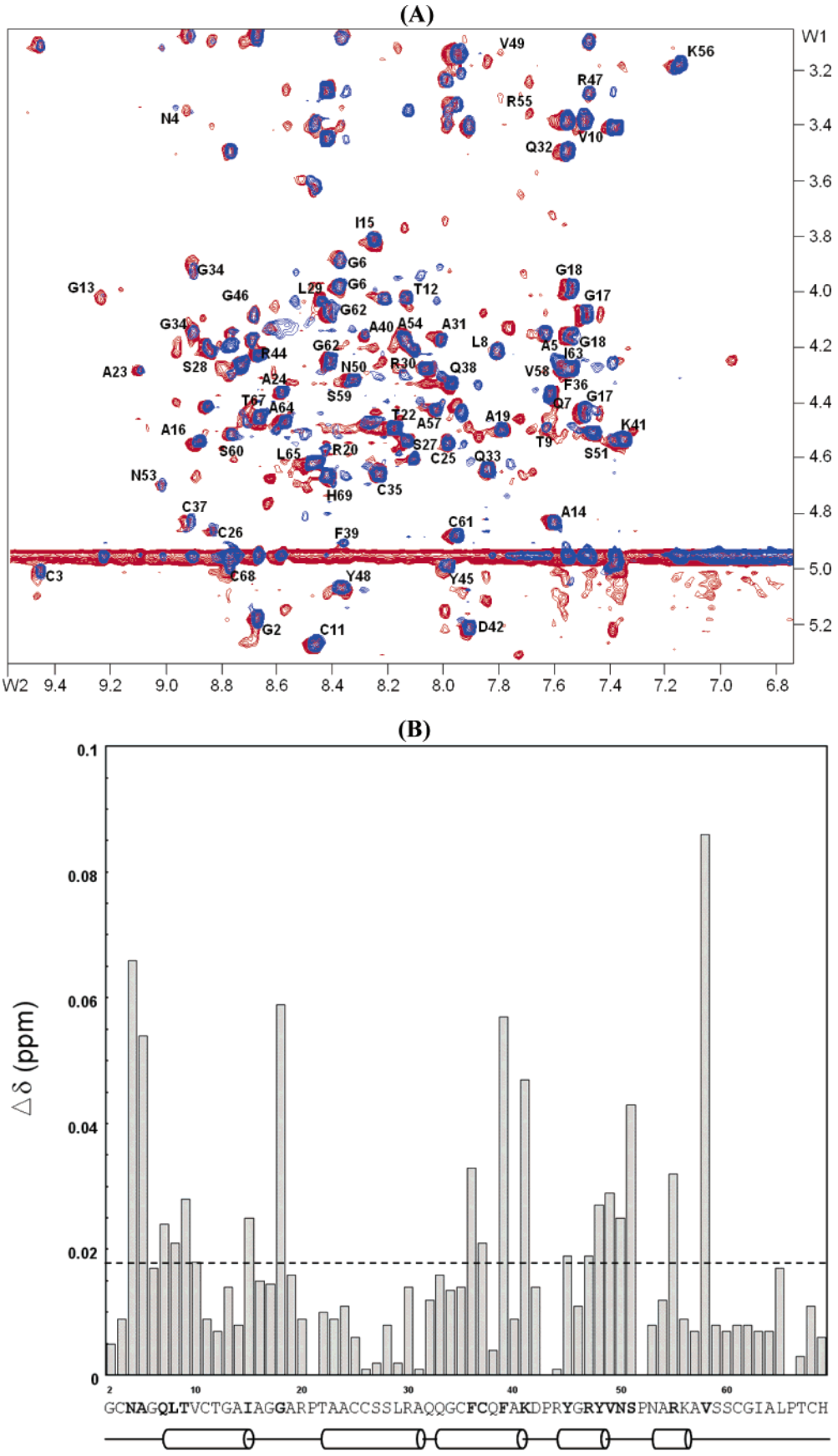

FIGURE 4: (A) Comparison of the fingerprint regions of ^{1}H TOCSY spectra. The peaks for free rice nsLTP2 are shown in blue, while the peaks for the cholesterol-bound complex form are shown in red. (B) A plot representing the sum of chemical shift perturbations ($\Delta\delta$) for each amino acid in the fingerprint region is used to locate various residues involved in the sterol binding. The residues having larger chemical shift perturbations are represented with bold letters in the protein sequence. A schematic diagram of the secondary structure of rice nsLTP2 is shown at the bottom, where helices are represented as cylinders.

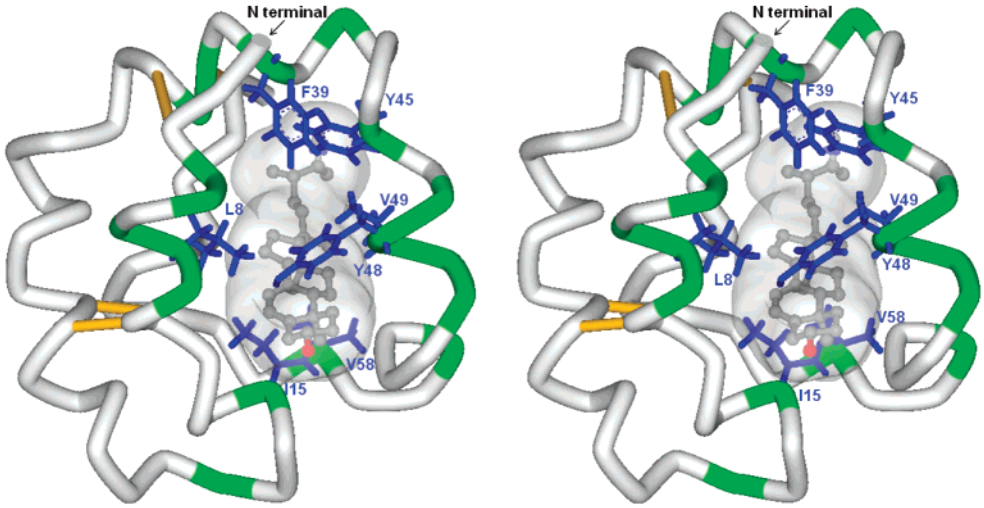

FIGURE 5: Stereoview of the nsLTP2/sterol complex. Various residues involved in the sterol binding are colored in green. Most of these residues are located around helices I, IV, and V. Comparing the theoretical docked structure and experimental NMR results, the residues directly interacting with the ligand are Leu[8], Ile[15], Phe[39], Tyr[45], Tyr[48], Val[49], and Val[58] labeled by blue stick representations. Cholesterol is shown in a ball and stick mode, while the tube style is used for nsLTP2. The disulfide bonds are colored in yellow.

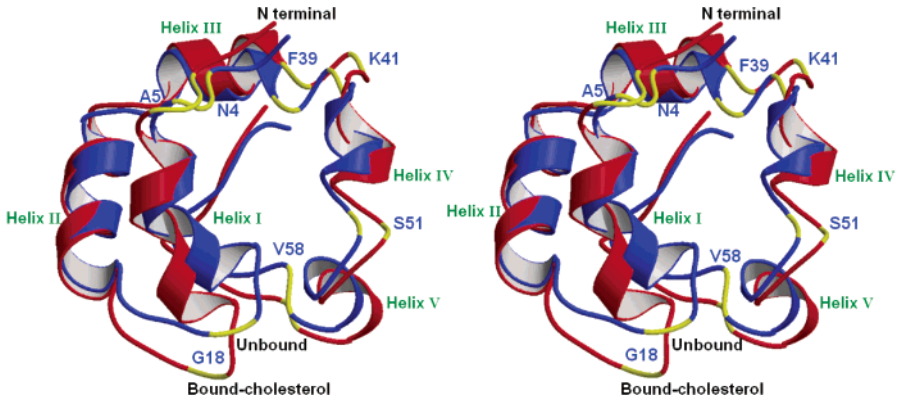

FIGURE 6: Superposition of the cholesterol complex (red) and free (blue) forms of rice nsLTP2 three-dimensional structures. The major difference in the two conformations is observed at the loop between helices I and II, where the structure is stretched out approximately 3.10 Å. Residues with larger chemical shift perturbations were also represented in yellow.

of rice nsLTP2. Insertion of cholesterol into rice nsLTP2 expanded the hydrophobic cavity from 132.55 to 325.59 Å^3. Likewise, the cavity volume of nsLTP2 also increased to 294.81 Å^3 for ergosterol binding. The change in the three-dimensional structures of rice nsLTP2 upon binding to cholesterol is illustrated in Figure 6 using the MolScript v2.1 representation (*51*). The sterol molecule is in close contact with helices I, IV, and V. The major difference in the two conformations is at the loop between helices I and II, where it is stretched by approximately 3.10 Å. The overall backbone atomic RMSD values measured with Swiss-Pdb Viewer v3.6 for cholesterol and ergosterol complexes compared to the ligand-free state are 1.57 and 2.03 Å (*52*). Similarly, the overall side chain atomic RMSDs for cholesterol and ergosterol complexes are 1.90 and 2.33 Å. As regards the change range of the backbone atomic RMSD for each residue, the maximum value for the complex and cholesterol-free states is 4.193 Å and the minimum value is 0.513 Å. In the case of ergosterol binding, the backbone atomic RMSDs for each residue are between 4.171 and 0.363 Å. Seven residues (Asn[4], Ala[5], Gly[18], Phe[39], Lys[41], Ser[51], and Val[58]) with larger chemical shift perturbations ($\Delta\sigma$ > 0.04 ppm) were also mapped in the structural alignment plot (Figure 6). Those residues labeled in the figure were mostly located at regions with a larger conformational change. The backbone atomic RMSD for these seven residues is approximately 2.24 Å, and the side chain atomic RMSD is 2.84 Å. It was suggested that cholesterol inserted into rice nsLTP2 to expand the hydrophobic cavity and then caused the structural change. The potential energy was also calculated using the CVFF force field. The protein-only structure (632.61 kcal mol^{-1}) is less stable than the structure of the cholesterol/protein complex (496.57 kcal mol^{-1}). Theoretical modeling and denaturant-induced unfolding studies were thus in agreement with respect to the stabilizing effect of sterol binding to nsLTP2. In addition, various residues involved in the cholesterol binding and crucial for complex formation are Leu[8], Ile[15], Phe[39], Tyr[45], Tyr[48], Val[49], Pro[52], Ala[54], Val[58], Leu[65], and Pro[66] according to Ligplot analysis (*40*). The side chains of the two tyrosines (Tyr[45] and Tyr[48]) shift to the inner cavity to interact with a ligand. The amide protons of Phe[39] and residues around helices I, IV, and V are involved in the new hydrogen bonds. These new bonds may change the overall deuterium uptake in the hydrogen/deuterium exchange experiment and provide contrasting values of protected hydrogens. Comparing the theoretical structure and experimental results, the residues directly interacting with the ligand are Leu[8], Ile[15], Phe[39], Tyr[45], Tyr[48], Val[49], and Val[58],

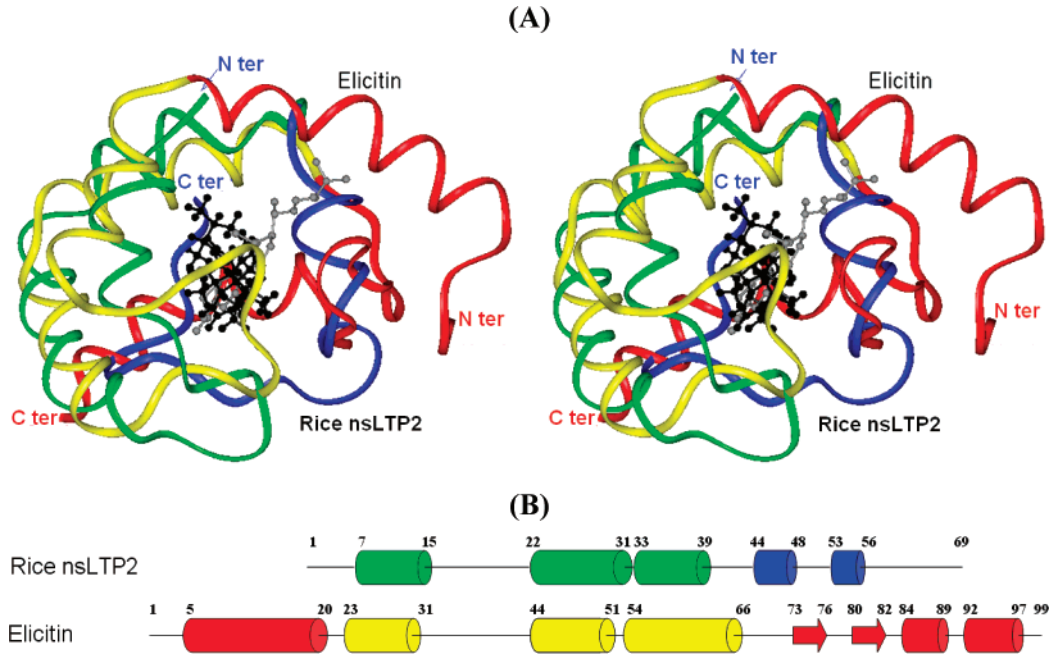

FIGURE 7: (A) Three-dimensional structural alignment of cryptogein and rice nsLTP2. Rice nsLTP2 and cryptogein share similar structural motifs. Rice nsLTP2 and cryptogein complexes have an L-shaped helical motif and a flexible loop region. The highly rigid portion of rice nsLTP2 (green) is closely aligned with cryptogein (yellow). The flexible region of rice nsLTP2 and the remaining portions of cryptogein are colored in blue and red, respectively. Ergosterol is shown with the ball and stick model with different colors for cryptogein-bound ergosterol (gray) and rice nsLTP2-bound sterol (black) molecules. (B) Schematic diagram of secondary structural alignment of cryptogein and rice nsLTP2. Closely aligned helical regions are represented with green (rice nsLTP2) and yellow (cryptogein) cylinders. Other cylinders and arrows represent other helices and β strands, respectively. The amino acid positions of various structural regions are labeled.

revealed with blue stick representations (Figure 5). The cholesterol molecule is shown with a ball and stick representation.

Comparison of Sterol Complexes with nsLTP2 and Elicitin. Although rice nsLTP2 and cryptogein share only 20% sequence identity, they display similar "L"-shaped helical motifs and flexible regions. The complexes of cryptogein and rice nsLTP2 with ergosterol were superimposed (a stereoview representation in Figure 7A). Helices I, II, and III of rice nsLTP2 (green) are perfectly aligned with helices II, III, and IV of cryptogein (yellow), respectively. The backbone atomic RMSD for these regions is 4.57 Å. The helical regions form an L-shaped framework to support the ergosterol association. The schematic representation of the secondary structural overlap of cryptogein and rice nsLTP2 is shown in Figure 7B. Ergosterol inserts into the nsLTP2 cavity in a fashion similar to that in the cryptogein/ergosterol complex, where many tyrosines, Tyr^{12}, Tyr^{33}, Tyr^{47}, and Tyr^{87}, are involved in the interaction (*21*). In the case of nsLTP2, Phe^{39}, Tyr^{45}, and Tyr^{48} are involved in ergosterol binding (Figure 5). Thus, aromatic side chains appear to play a similarly crucial role in ergosterol association in these complexes.

Accommodation of sterol molecules in elicitin is an essential step for recognition of the receptor at the plant membrane to trigger the plant defense (*53*). Plant nsLTP1 has a high affinity for biological receptors recognized by the elicitin/sterol complex but failed to trigger the signaling pathway (*22*). A consensus is emerging that association of a hydrophobic ligand is essential for nsLTPs to induce defense responses (*20*). Although nsLTP1 shares structural similarities with elicitin, it failed to accommodate rigid sterol molecules (*20*, *22*). The endogenous nsLTP2 associated with a sterol molecule might interact with the plant membrane receptor to induce a cellular signal pathway and promote plant defense responses to inhibit or kill the microbes. Our results provide a rationale for further exploration of the mechanism of nsLTP2 in plant defense.

Comparison of nsLTP1 with nsLTP2. NsLTP1 and nsLTP2 are all helical basic proteins that show 30% sequence similarities. Although nsLPT1 recognized the elicitin/sterol receptor at the plant surface, it failed to induce plant defense (*22*). A recent report suggested that the gene essential for plant defense is nsLTP2 (*23*). To understand the discrepancy involved in their mechanisms, the structures and modes of ligand binding were analyzed. The backbone atomic RMSD for rice nsLTP1 (PDB code 1RZL) with rice nsLTP2 (PDB code 1L6H) shows a lower value (2.21 Å) because the basic framework is supported by four well-conserved disulfide bonds. The size of the hydrophobic cavity for rice nsLTP1 (366.5 $Å^3$) is larger than that for rice nsLTP2 (132.55 $Å^3$). Despite the cavity size, nsLTP2 but not nsLTP1 could accommodate a rigid sterol molecule (Figure 1B). The plasticity of the hydrophobic cavity and flexibility of the hydrophobic molecules are necessary for binding (*20*). Thus, the preference for rigid molecules is not attributed to the protein's cavity size but its mode of binding. The conformation of nsLTP2 includes a long flexible region at one side of the molecule and a disulfide-bonded rigid helical portion on the other. Cholesterol insertion through the highly flexible portion of nsLTP2 posed little spatial restriction. The disulfide bonds serve as hinges, as shown as yellow sticks in Figure 5, to accommodate cholesterol molecule binding to nsLTP2. NsLTP2 is opened up like a shell to form hydrophobic contacts with the ligand. Because nsLTP1 would require unrealistic distortion to accommodate the perhydro-1, 2-cyclopentanophenanthrene ring system, it can only bind to linear lipid molecules (Figure 1B) (*6*, *7*, *10*). In the case

of nsLTP1, disulfide bonds connect four helices to form a tunnel-like hydrophobic cavity and restrict spatial flexibility. As a consequence, nsLTP1 is only able to accommodate linear lipid molecules such as fatty acids and not rigid voluminous molecules.

CONCLUSION

Both theoretical simulation and experimental data suggest that regardless of the cavity size, rice nsLTP2 but not nsLTP1 could bind to a rigid sterol molecule. The disulfide bonds of nsLTP1 may restrict the flexibility of the protein to accommodate sterol molecules. The nsLTP2 conformation is minimally perturbed upon sterol binding, and tyrosine residues adjacent to the hydrophobic cavity mediate the protein/hydrophobic ligand interaction. Elicitins secreted by a fungal pathogen must associate with sterol molecules to be recognized by the receptor at the plant membrane to induce a signaling pathway. Although nsLTP1 has a high affinity for elicitin receptors, it is unable to prompt defense mechanisms (*22*). It is suggested that association of sterol molecules is a critical step for elicitins or nsLTPs to bind to a receptor involved in the control of plant defense responses (*20*). NsLTP1 has high structural similarities with elicitin, but it is unable to accommodate sterol molecules. Our results showed that nsLTP2 can bind not only lipids but also sterol molecules. Furthermore, these nsLTP2/sterol complexes may interact with receptors at plant plasma membranes to trigger plant defense responses.

REFERENCES

1. Jegou, S., Douliez, J. P., Molle, D., Boivin, P., and Marion, D. (2000) Purification and structural characterization of LTP1 polypeptides from beer, *J. Agric. Food Chem. 48*, 5023−9.
2. Douliez, J. P., Pato, C., Rabesona, H., Molle, D., and Marion, D. (2001) Disulfide bond assignment, lipid transfer activity and secondary structure of a 7-kDa plant lipid transfer protein, LTP2, *Eur. J. Biochem. 268*, 1400−3.
3. Kader, J. C. (1996) Lipid-transfer proteins in plants, *Annu. Rev. Plant Physiol. Plant Mol. Biol. 47*, 627−54.
4. Liu, Y. J., Samuel, D., Lin, C. H., and Lyu, P. C. (2002) Purification and characterization of a novel 7-kDa non-specific lipid transfer protein-2 from rice (Oryza sativa), *Biochem. Biophys. Res. Commun. 294*, 535−40.
5. Shin, D. H., Lee, J. Y., Hwang, K. Y., Kim, K. K., and Suh, S. W. (1995) High-resolution crystal structure of the non-specific lipid-transfer protein from maize seedlings, *Structure 3*, 189−99.
6. Lee, J. Y., Min, K., Cha, H., Shin, D. H., Hwang, K. Y., and Suh, S. W. (1998) Rice non-specific lipid transfer protein: the 1.6 Å crystal structure in the unliganded state reveals a small hydrophobic cavity, *J. Mol. Biol. 276*, 437−48.
7. Han, G. W., Lee, J. Y., Song, H. K., Chang, C., Min, K., Moon, J., Shin, D. H., Kopka, M. L., Sawaya, M. R., Yuan, H. S., Kim, T. D., Choe, J., Lim, D., Moon, H. J., and Suh, S. W. (2001) Structural basis of non-specific lipid binding in maize lipid-transfer protein complexes revealed by high-resolution X-ray crystallography, *J. Mol. Biol. 308*, 263−78.
8. Samuel, D., Liu, Y. J., Cheng, C. S., and Lyu, P. C. (2002) Solution structure of plant nonspecific lipid transfer protein-2 from rice (Oryza sativa), *J. Biol. Chem. 277*, 35267−73.
9. Pons, J. L., de Lamotte, F., Gautier, M. F., and Delsuc, M. A. (2003) Refined solution structure of a liganded type 2 wheat nonspecific lipid transfer protein, *J. Biol. Chem. 278*, 14249−56.
10. Lerche, M. H., Kragelund, B. B., Bech, L. M., and Poulsen, F. M. (1997) Barley lipid-transfer protein complexed with palmitoyl CoA: the structure reveals a hydrophobic binding site that can expand to fit both large and small lipid-like ligands, *Structure 5*, 291−306.
11. Douliez, J. P., Michon, T., Elmorjani, K., and Marion, D. (2000) Structure, biological and technological functions of lipid transfer proteins and indolines, the major lipid binding proteins from cereal kernels, *J. Cereal Sci. 32*, 1−20.
12. Pato, C., Tran, V., Marion, D., and Douliez, J. P. (2002) Effects of acylation on the structure, lipid binding, and transfer activity of wheat lipid transfer protein, *J. Protein Chem. 21*, 195−201.
13. Tassin, S., Broekaert, W. F., Marion, D., Acland, D. P., Ptak, M., Vovelle, F., and Sodano, P. (1998) Solution structure of Ace-AMP1, a potent antimicrobial protein extracted from onion seeds. Structural analogies with plant nonspecific lipid transfer proteins, *Biochemistry 37*, 3623−37.
14. Garcia-Olmedo, F., Molina, A., Segura, A., and Moreno, M. (1995) The defensive role of nonspecific lipid-transfer proteins in plants, *Trends Microbiol. 3*, 72−4.
15. Selitrennikoff, C. P. (2001) Antifungal proteins, *Appl. Environ. Microbiol. 67*, 2883−94.
16. Ponchet, M., Panabieres, F., Milat, M. L., Mikes, V., Montillet, J. L., Suty, L., Triantaphylides, C., Tirilly, Y., and Blein, J. P. (1999) Are elicitins cryptograms in plant-Oomycete communications? *Cell. Mol. Life Sci. 56*, 1020−47.
17. Mikes, V., Milat, M. L., Ponchet, M., Ricci, P., and Blein, J. P. (1997) The fungal elicitor cryptogein is a sterol carrier protein, *FEBS Lett. 416*, 190−2.
18. Mikes, V., Milat, M. L., Ponchet, M., Panabieres, F., Ricci, P., and Blein, J. P. (1998) Elicitins, proteinaceous elicitors of plant defense, are a new class of sterol carrier proteins, *Biochem. Biophys. Res. Commun. 245*, 133−9.
19. Hartmann, M.-A. (1998.) Plant sterols and the membrane environment, *Trends Plant Sci. 3*, 170−75.
20. Blein, J. P., Coutos-Thevenot, P., Marion, D., and Ponchet, M. (2002) From elicitins to lipid-transfer proteins: a new insight in cell signalling involved in plant defence mechanisms, *Trends Plant Sci. 7*, 293−6.
21. Boissy, G., O'Donohue, M., Gaudemer, O., Perez, V., Pernollet, J. C., and Brunie, S. (1999) The 2.1 Å structure of an elicitin-ergosterol complex: a recent addition to the Sterol Carrier Protein family, *Protein Sci. 8*, 1191−9.
22. Buhot, N., Douliez, J. P., Jacquemard, A., Marion, D., Tran, V., Maume, B. F., Milat, M. L., Ponchet, M., Mikes, V., Kader, J. C., and Blein, J. P. (2001) A lipid transfer protein binds to a receptor involved in the control of plant defence responses, *FEBS Lett. 509*, 27−30.
23. Maldonado, A. M., Doerner, P., Dixon, R. A., Lamb, C. J., and Cameron, R. K. (2002) A putative lipid transfer protein involved in systemic resistance signalling in Arabidopsis, *Nature 419*, 399−403.
24. Gomes, E., Sagot, E., Gaillard, C., Laquitaine, L., Poinssot, B., Sanejouand, Y. H., Delrot, S., and Coutos-Thevenot, P. (2003) Nonspecific lipid-transfer protein genes expression in grape (Vitis sp.) cells in response to fungal elicitor treatments, *Mol. Plant-Microbe Interact. 16*, 456−64.
25. Yu, Y. G., Chung, C. H., Fowler, A., and Suh, S. W. (1988) Amino acid sequence of a probable amylase/protease inhibitor from rice seeds, *Arch. Biochem. Biophys. 265*, 466−75.
26. Smutzer, G., Crawford, B. F., and Yeagle, P. L. (1986) Physical properties of the fluorescent sterol probe dehydroergosterol, *Biochim. Biophys. Acta 862*, 361−71.
27. Zhou, H. X., Lyu, P., Wemmer, D. E., and Kallenbach, N. R. (1994) Alpha helix capping in synthetic model peptides by reciprocal side chain-main chain interactions: evidence for an N terminal "capping box", *Proteins 18*, 1−7.
28. Demmers, J. A., Haverkamp, J., Heck, A. J., Koeppe, R. E., II, and Killian, J. A. (2000) Electrospray ionization mass spectrometry as a tool to analyze hydrogen/deuterium exchange kinetics of transmembrane peptides in lipid bilayers, *Proc. Natl. Acad. Sci. U.S.A. 97*, 3189−94.
29. Demmers, J. A., van Duijn, E., Haverkamp, J., Greathouse, D. V., Koeppe, R. E., 2nd, Heck, A. J., and Killian, J. A. (2001) Interfacial positioning and stability of transmembrane peptides in lipid bilayers studied by combining hydrogen/deuterium exchange and mass spectrometry, *J. Biol. Chem. 276*, 34501−8.
30. Dubreil, L., Compoint, J. P., and Marion, D. (1997) Interaction of Puroindolines with Wheat Flour Polar Lipids Determines Their Foaming Properties, *J. Agric. Food Chem. 45*, 108−16.
31. Lascombe, M. B., Ponchet, M., Venard, P., Milat, M. L., Blein, J. P., and Prange, T. (2002) The 1.45 Å resolution structure of the cryptogein-cholesterol complex: a close-up view of a sterol

carrier protein (SCP) active site, *Acta Crystallogr., D: Biol. Crystallogr. 58*, 1442−7.
32. Lascombe, M. B., Milat, M. L., Blein, J. P., Panabieres, F., Ponchet, M., and Prange, T. (2000) Crystallization and preliminary X-ray studies of oligandrin, a sterol-carrier elicitor from Pythium oligandrum, *Acta Crystallogr., D: Biol. Crystallogr. 56* (Part 11), 1498−500.
33. Goddard, T. D., and Kneller, D. G. (1999) SPARKY 3, University of California, San Francisco.
34. Sachchidanand, Lequin, O., Staunton, D., Mulloy, B., Forster, M. J., Yoshida, K., and Campbell, I. D. (2002) Mapping the heparin-binding site on the 13-14F3 fragment of fibronectin, *J. Biol. Chem. 277*, 50629−35.
35. Crowley, P. B., Diaz-Quintana, A., Molina-Heredia, F. P., Nieto, P., Sutter, M., Haehnel, W., De La Rosa, M. A., and Ubbink, M. (2002) The interactions of cyanobacterial cytochrome c6 and cytochrome f, characterized by NMR, *J. Biol. Chem. 277*, 48685−9.
36. Vakser, I. A., Matar, O. G., and Lam, C. F. (1999) A systematic study of low-resolution recognition in protein−protein complexes, *Proc. Natl. Acad. Sci. U.S.A. 96*, 8477−82.
37. Vakser, I. A., and Aflalo, C. (1994) Hydrophobic docking: a proposed enhancement to molecular recognition techniques, *Proteins 20*, 320−9.
38. Katchalski-Katzir, E., Shariv, I., Eisenstein, M., Friesem, A. A., Aflalo, C., and Vakser, I. A. (1992) Molecular surface recognition: determination of geometric fit between proteins and their ligands by correlation techniques, *Proc. Natl. Acad. Sci. U.S.A. 89*, 2195−9.
39. Khurana, S., Sanli, G., Powers, D. B., Anderson, S., and Blaber, M. (2000) Molecular modeling of substrate binding in wild-type and mutant Corynebacteria 2,5-diketo-D-gluconate reductases, *Proteins 39*, 68−75.
40. Wallace, A. C., Laskowski, R. A., and Thornton, J. M. (1995) LIGPLOT: a program to generate schematic diagrams of protein−ligand interactions, *Protein Eng. 8*, 127−34.
41. Kleywegt, G. J., and Jones, T. A. (1994) Detection, delineation, measurement and display of cavities in macromolecular structures, *Acta Crystallogr. D50*, 178−85.
42. Jean-Charles, A., Nicholls, A., Sharp, K., Honig, B., Tempczyk, A., Hendrickson, T. H., and Clark, W. (1991) Electrostatic Contributions to Solvation Energies: Comparisons of Free Energy Perturbation and Continuum Calculations, *J. Am. Chem. Soc. 113*, 1454−1454.
43. Lindorff-Larsen, K., and Winther, J. R. (2001) Surprisingly high stability of barley lipid transfer protein, LTP1, towards denaturant, heat and proteases, *FEBS Lett. 488*, 145−8.
44. Kamal, J. K., and Behere, D. V. (2002) Thermal and conformational stability of seed coat soybean peroxidase, *Biochemistry 41*, 9034−42.
45. Greene, R. F., Jr., and Pace, C. N. (1974) Urea and guanidine hydrochloride denaturation of ribonuclease, lysozyme, alpha-chymotrypsin, and beta-lactoglobulin, *J. Biol. Chem. 249*, 5388−93.
46. Santoro, M. M., and Bolen, D. W. (1988) Unfolding free energy changes determined by the linear extrapolation method. 1. Unfolding of phenylmethanesulfonyl alpha-chymotrypsin using different denaturants, *Biochemistry 27*, 8063−8.
47. Englander, S. W., Sosnick, T. R., Englander, J. J., and Mayne, L. (1996) Mechanisms and uses of hydrogen exchange, *Curr. Opin. Struct. Biol. 6*, 18−23.
48. Deng, Y., Zhang, Z., and Smith, D. L. (1999) Comparison of continuous and pulsed labeling amide hydrogen exchange/mass spectrometry for studies of protein dynamics, *J. Am. Soc. Mass Spectrom. 10*, 675−84.
49. Nemirovskiy, O., Giblin, D. E., and Gross, M. L. (1999) Electrospray ionization mass spectrometry and hydrogen/deuterium exchange for probing the interaction of calmodulin with calcium, *J. Am. Soc. Mass Spectrom. 10*, 711−8.
50. Wuthrich, K. (1986) *NMR of Proteins and Nucleic Acids*, J. Wiley & Sons, New York.
51. Kraulis P. J. (1991) MOLSCRIPT: A Program to Produce Both Detailed and Schematic Plots of Protein Structures, *J. Appl. Crystallogr. 24*, 946−50.
52. Guex, N., and Peitsch, M. C. (1997) SWISS-MODEL and the Swiss-PdbViewer: an environment for comparative protein modeling, *Electrophoresis 18*, 2714−23.
53. Osman, H., Vauthrin, S., Mikes, V., Milat, M. L., Panabieres, F., Marais, A., Brunie, S., Maume, B., Ponchet, M., and Blein, J. P. (2001) Mediation of elicitin activity on tobacco is assumed by elicitin-sterol complexes, *Mol. Biol. Cell 12*, 2825−34.

BI048873J